Chemosphere 303 (2022) 134949

Contents lists available at ScienceDirect

Chemosphere

journal homepage: www.elsevier.com/locate/chemosphere

The state of the art review on photocatalytic Cr(VI) reduction over MOFs-based photocatalysts: From batch experiment to continuous operation

Chong-Chen Wang [a,b,*], Xueying Ren [a,b], Peng Wang [a,b], Cheng Chang [c]

[a] Beijing Key Laboratory of Functional Materials for Building Structure and Environment Remediation, Beijing University of Civil Engineering and Architecture, Beijing, 100044, China

[b] Beijing Energy Conservation & Sustainable Urban and Rural Development Provincial and Ministry Co-construction Collaboration Innovation Center, Beijing University of Civil Engineering and Architecture, Beijing, 100044, China

[c] School of Engineering and Physical Sciences, Heriot-Watt University, Edinburgh, EH14 4AS, UK

HIGHLIGHTS

- The Cr(VI) reduction in MOF-based photocatalysts in past 5 years were summarized.
- The continuous Cr(VI) reduction can be achieved via the immobilized MOFs.
- The prospective of Cr(VI) reduction in MOF-based photocatalysts is declared.

GRAPHICAL ABSTRACT

ARTICLE INFO

Handling Editor: Jun Huang

Keywords:
Metal-organic frameworks
Photocatalytic reduction
Hexavalent chromium
Environmental application
Continuous operation

ABSTRACT

This state of the art review presented the photocatalytic reduction from highly toxic Cr(VI) to lowly toxic Cr(III) with metal-organic frameworks (MOFs) and their composites. The construction of composites facilitated the transportation of the photo-induced charges to enhance the Cr(VI) reduction, in which the corresponding mechanisms were clarified by both experimental tests and DFT calculations. The immobilized MOFs onto some substrates accomplished continuous operations toward Cr(VI) reduction even under real solar light. As well, the environmental applications of the Cr(VI) reduction were analyzed, in which the influence factors toward the Cr (VI) reduction were clarified. This review reported that a big breakthrough was achieved from the batch experiment to the continuous operation for Cr(VI) reduction, in which MOFs demonstrated a bright prospective in the field of photocatalytic Cr(VI) reduction.

* Corresponding author. Beijing Key Laboratory of Functional Materials for Building Structure and Environment Remediation, Beijing University of Civil Engineering and Architecture, Beijing, 100044, China.

E-mail addresses: wangchongchen@bucea.edu.cn, chongchenwang@126.com (C.-C. Wang).

https://doi.org/10.1016/j.chemosphere.2022.134949
Received 29 March 2022; Received in revised form 4 May 2022; Accepted 10 May 2022
Available online 13 May 2022

1. Introduction

Some metal-organic frameworks (MOFs) including but not limited to UiO-66, MIL-125, MOF-5 are deemed as ideal photocatalyst candidates (Wang et al., 2014; Zeng et al., 2016), in which the organic ligands and metal-oxo clusters act as the light-absorbing antenna and isolated semiconductor quantum dots, respectively (Wang and Ho, 2016; Wang et al., 2020). The metal templates, organic linkers, channels or pores in the MOFs frameworks can be easily tuned due to the intrinsic modular property of the MOFs (Wang et al., 2020). Especially, the well-defined crystal structures of MOFs can be obtained from the single crystals via the X-ray diffraction technology, which can be used to clarify the structure-activity relationship (Wang et al., 2022; Zhao et al., 2021a). Therefore, the MOFs-based photocatalysts attracted increasing interests in various research fields like H_2 and O_2 production from water splitting (Ali et al., 2021; Cai et al., 2017), CO_2 reduction (Wang et al., 2015a), organic pollutants degradation (Yi et al., 2021; Zhao et al., 2022), antimicrobial (Li et al., 2021a) and Cr(VI) reduction (Gao et al., 2019; He et al., 2021; Wang et al., 2016).

Considering that the MOFs constructed from the hard metals (like Zr^{4+}, Ti^{4+} and Fe^{3+}) and polycarboxylic acids (like terephthalic acid, trimesic acid and fumaric acid) can be stable under acidic solutions, they are often adopted as photocatalysts to accomplish photocatalytic hexavalent chromium Cr(VI) reduction (Wang et al., 2019). As well known, all Cr(VI) compounds are highly toxic considering their high water solubility and carcinogenic impact toward most organisms (Chen et al., 2021; Kaur et al., 2021), which can be reduced into Cr(III) to low the toxicity and to increase the precipitation (Wei et al., 2016; Yao et al., 2014; Zhang et al., 2015). Among the different Cr(VI) sequestration methods like chemical reduction, photocatalytic reduction displayed some advantages like convenient utilization of solar light, less or even no secondary pollution, as well as lower cost, which is preferred to be used for the removal of Cr(VI) pollutants in water (Li et al., 2018; Zhang et al., 2018b; Zhang et al., 2013).

In 2016, we published a mini review paper to present the research progress of the Cr(VI) reduction with the help of MOFs photocatalysts (Wang et al., 2016), which attracted massive attentions from our worldwide counterparts. In the past five years, some significant research findings concerning the photocatalytic Cr(VI) reduction adopting MOFs and MOFs-based materials as photocatalysts emerged. Also, some review papers concerning Cr(VI) reduction were published, in which the corresponding research status and outlook were proposed as from different views (Kumar et al., 2021; Li et al., 2021; Zhao et al., 2019). In recent years, our research group focused on the photocatalytic Cr(VI) reduction over MOFs-based materials ranging from new pristine MOFs to different MOFs composites constructed from different secondary or ternary components. Especially, we proposed to accomplish continuous Cr(VI) reduction over the immobilized MOFs photocatalysts under artificial UV/visible light and even real solar light. Therefore, it was essential to present the updated review paper based on our corresponding research results for providing insightful summary and prospective, aiming to promote the large-scale applications in the real scenarios.

2. From individual MOFs to their composites

2.1. The new pristine MOFs as photocatalysts for Cr(VI) reduction

Inspired by the typical MOFs photocatalysts like NH_2-MIL-125(Ti) (Wang et al., 2015b), NH_2-UiO-66(Zr) (Shen et al., 2015; Shen et al., 2013a), NH_2-MIL-88 B(Fe) (Shi et al., 2015), NH_2-MIL-53(Fe) (Liang et al., 2015a), NH_2-MIL-68(In) (Liang et al., 2015b) and NH_2-MIL-101 (Fe) (Shi et al., 2015) for Cr(VI) reduction, some new approaches to enhance the photocatalytic Cr(VI) reduction were proposed. For example, Wang and coworkers fabricated $(OH)_2$-UiO-66-X% via introducing 2,5-dihydroxyterephthalic acid to partially replace benzene-1,4-dicarboxylic acid (Li et al., 2021b), due to that the introduction of –OH groups could harvest light with longer wavelength, narrow the band gap as well as enhance the separation of charge carriers (Xie et al., 2020). In this work, tartaric acid was adopted not only as electron transfer medium to produce $COO^{\cdot-}$ radicals for boosting the Cr(VI) reduction but also as hole capture agent to enhance the separation of the photo-yielded electron-hole pairs (Fig. 1). Besides the classic MOFs, some new MOFs photocatalysts like BUC-20 (Zhong et al., 2019), BUC-21 (Wang et al., 2017), BUC-66/67 (Yi et al., 2018), BUC-85/86 (Ma et al., 2020), NNU-36 (Zhao et al., 2017) and so on (Guo et al., 2020; Kaur et al., 2020; Xie et al., 2020; Zheng et al., 2019) were designed and synthesized for the purpose of photocatalytic Cr(VI) reduction.

Among these newly developed MOFs, BUC-21, a water stable 2D MOF constructed from *cis*-1,3-dibenzyl-2-imidazolidone-4,5-dicarboxylic acid, 4,4′-bipyridine and Zn^{2+}, displayed the outstanding photocatalysis performance under the irradiation of UV light (Wang et al., 2017), due to that *cis*-1,3-dibenzyl-2-imidazolidone-4,5-dicarboxylic acid is an excellent light responsive organic linker. BUC-21 could accomplish 96% Cr(VI) reduction with initial $K_2Cr_2O_7$ concentration of 10.0 mg/L (pH = 2.0) within 30.0 min under UV light, which was superior to the P25's (a commercial TiO_2) performance (only 39.0%) under the identical condition. Upon the irradiation of UV light, the photoinduced electrons were produced over the lowest unoccupied molecular orbital (LUMO) to reduce Cr(VI) into Cr(III). To enhance the Cr(VI) reduction via boosted separation of electron-hole pairs, the reactive red X–3B (X–3B) was selected as organic pollutant to consume the left holes over the highest occupied molecular orbital (HOMO) due to that BUC-21 can accomplish effectively photocatalytic degradation toward several organic dyes like methylene blue (MB), rhodamine B (RhB), methyl orange (MO) and X–3B under UV light. However, both Cr (VI) reduction and X–3B degradation activities decreased toward the matrix of Cr(VI) and X–3B with the identical conditions. In this system, the X–3B was primarily oxidized by $\cdot O_2^-$ radicals rather than holes, in which the $\cdot O_2^-$ radicals were formed via the reaction between the electrons and dissolved oxygen (DO). As the presence of both Cr(VI) and X–3B, the photo-induced electrons preferred to participate in the Cr(VI) reduction, which inhibited the formation of $\cdot O_2^-$ radicals responsible to X–3B oxidation.

It was generally believed that the $–NH_2$ groups in the ligand of the MOFs can accomplish visible light response and boosted separation of photo-induced electron-hole pair. For example, UiO-66 with band energy of 3.9 eV (HOMO: 3.35 eV and LUMO: 0.55 eV) can only be activated by UV light. However, the NH_2-UiO-66 can be activated by visible light due to the narrower band energy of 2.52 eV (HOMO: 2.01 eV and LUMO: 0.51 eV). As well, the $(OH)_2$-UiO-66 arose increasing interest due to that the introduced –OH groups can act as the intramolecular hole scavenger to enhance the quick separation of the photogenerated charge carrier (Li et al., 2021bLi et al., 2021b, 2021). However, the pristine $(OH)_2$-UiO-66 suffered from the unregular morphology (Fig. 1a) (Xie et al., 2020). Our group proposed an approach to prepare $(OH)_2$-UiO-66-X% (X represented the mole ratio of the introduced 2, 5-dihydroxyterephthalic acid) with mixed ligands of terephthalic acid and 2,5-dihydroxyterephthalic acid, in which the octahedral $(OH)_2$-UiO-66-20% with the particle size ranging from 1300 nm to 1500 nm displayed outstanding photocatalytic Cr(VI) reduction under 369 nm UV light provided by low power 10 W LED light source (Fig. 1b). The $(OH)_2$-UiO-66-20% displayed superior photocatalysis performance to the counterparts, in which the Cr(VI) with initial concentration of 10 mg/L can be completely reduced into Cr(III) at pH = 2.0 within 40.0 min. Tartaric acid (TA) as typical small molecular organic acid was adopted to further improve the Cr(VI) reduction performance. Without the addition of TA, the photo-induced electrons can reduce Cr(VI) via both direct electron transfer and via indirect electron transfer of forming $\cdot O_2^-$ radicals after reaction with dissolved oxygen (DO) (Fig. 1c). Beside the above-mentioned direct and indirect electron transfer mechanisms,

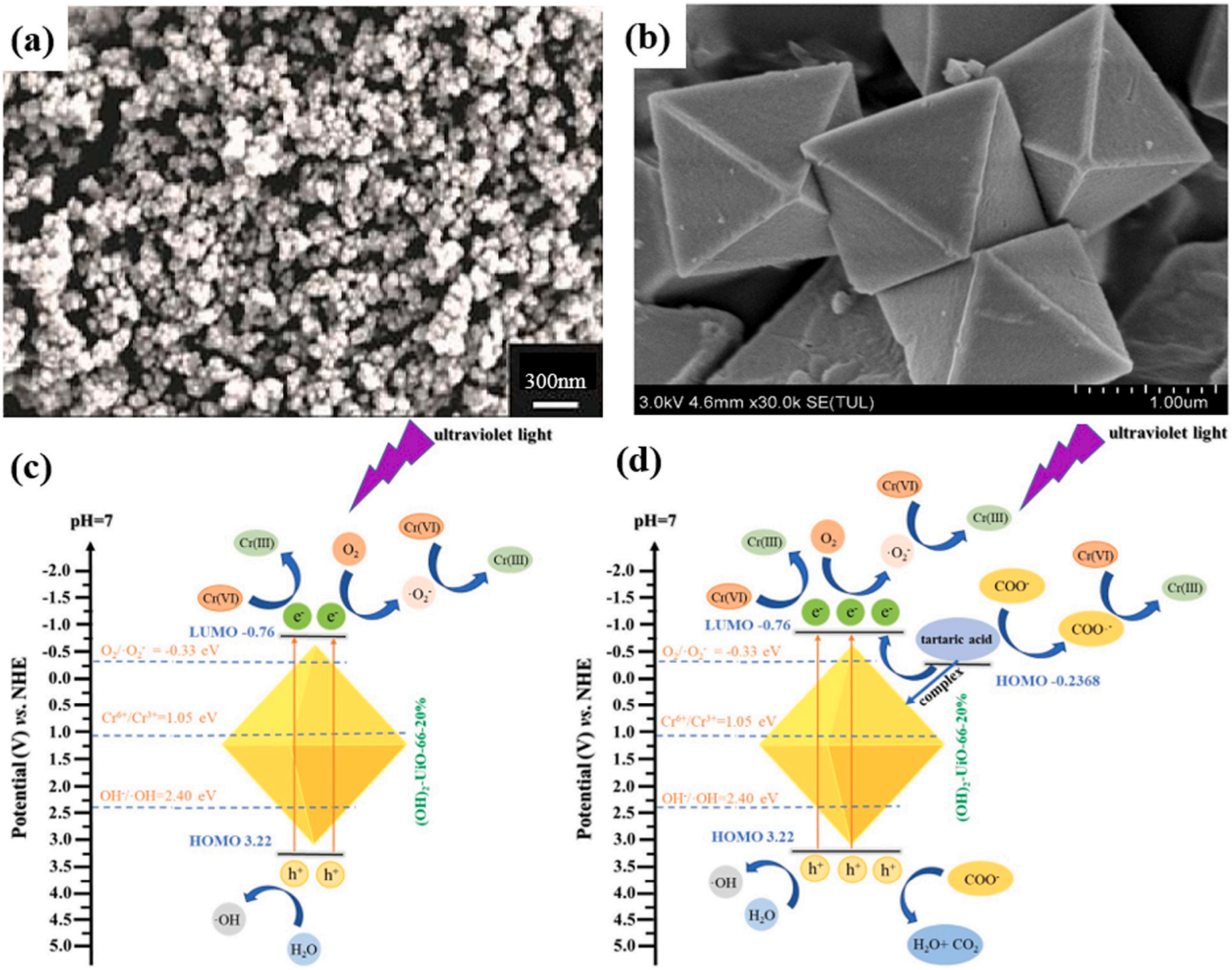

Fig. 1. SEM image of (a) $(OH)_2$-UiO-66 (Xie et al., 2020) and (b) $(OH)_2$-UiO-66-20% (Li et al., 2021b). The proposed mechanisms of Cr(VI) reduction in $(OH)_2$-UiO-66-20% (c) without the presence and (d) with the presence of tartaric acid (Li et al., 2021b).

the presence of TA can (i) consume the formed holes in HOMO to improve the electron-hole separation, (ii) react with $(OH)_2$-UiO-66-20% photocatalyst to yield charge-transfer-complex (CTC) for accelerate electron transfer, and (iii) form $COO^{\cdot}$ radicals to boost the Cr(VI) reduction (Fig. 1d). This work made it possible to prepare surface modified MOF photocatalysts, and to enhance the photocatalysis performance via the addition of suitable small molecular organic acid for practical applications.

2.2. The MOFs composites as photocatalysts for Cr(VI) reduction

Due to that the individual MOFs suffered from their poor electronic conductivity, rapid photo-induced charge carrier recombination, and limited light absorption utilization ability (Chen et al., 2020b; Li et al., 2021; Wang et al., 2014, 2016), it was a feasible and effective approach to combine MOFs with some highly conductive semiconductors or conductors like *g*-C_3N_4 (Du et al., 2019; Gao et al., 2019; Yi et al., 2019), WO_3 (Wang et al., 2021b), TiO_2-based semiconductors (Li et al., 2020b), bismuth-based semiconductors (Guo et al., 2020; Zhao et al., 2021b; Zhao et al., 2020a), Ag-based semiconductors (Zhou et al., 2020a; Zhou et al., 2019), *N*–$K_2Ti_4O_9$ (He et al., 2021), $Cd_{0.5}Zn_{0.5}S$ (Wei et al., 2020) PTCDA (3,4,9,10-perylenetetracarboxylic dianhydride) (Wei et al., 2021), and PANI (polyaniline) (Chen et al., 2020a) with good light-harvesting activity. It was believed that the introduction of some secondary or even ternary component to fabricate the composites with MOFs can also improve their stability (Ding et al., 2019), which can widen their potential applications (Wu et al., 2021).

Up to now, type-II and Z-scheme heterojunctions, as two mainstream heterojunctions, were widely explored (Wang et al., 2020; Xu et al., 2020). Generally, it was possible to design the expected heterojunctions type considering the conduction bands (CB) and valence bands (VB) positions of both components based on the perceived photoinduced charge transfer pathway (Huang et al., 2017; Zhao et al., 2021a). For example, considering that the CB of NH_2-UiO-66 and S–TiO_2 were determined as −0.60 eV and −0.35 eV vs. NHE and the VB potentials were calculated as 2.30 eV and 2.84 eV vs. NHE (Li et al., 2020b), it can be expected to construct type II S–TiO_2/NH_2-UiO-66 heterojunction as illustrated in Fig. 2a, which was confirmed by the determination of the photo-produced active species. The as-prepared S–TiO_2/NH_2-UiO-66 can photocatalytically reduce the Cr(VI) into Cr(III) primarily by the photo-yielded electrons accumulated on the CB of S–TiO_2, and secondarily by $\cdot O_2^-$ radicals. And the S–TiO_2/NH_2-UiO-66 can also oxidate bisphenol A (BPA) into small molecules with the aid of holes accumulated on the HOMO of NH_2-UiO-66 and the formed $\cdot O_2^-$ radicals on the CB of S–TiO_2 (Fig. 2a).

Things are not always what they happened. For example, the type II

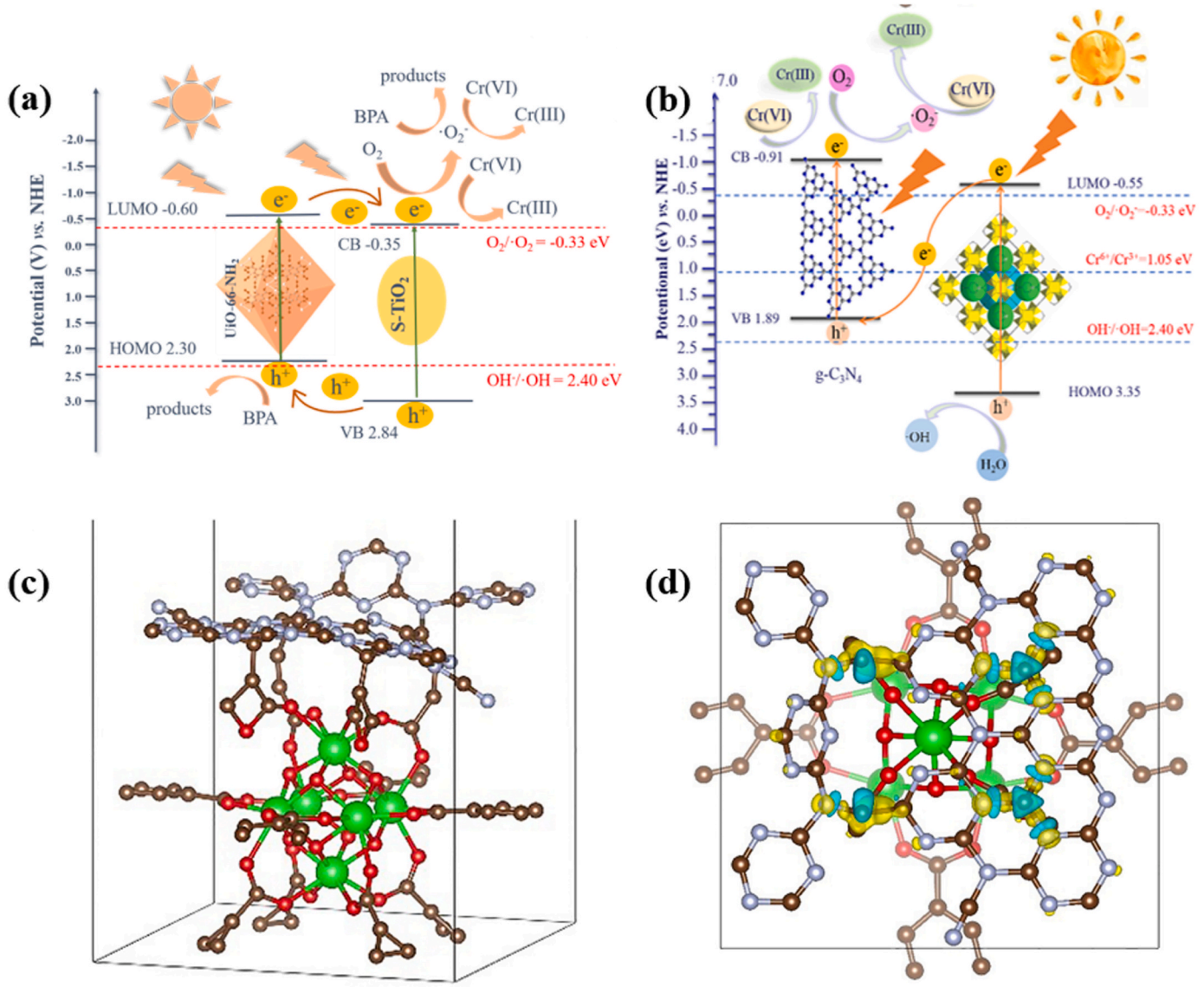

Fig. 2. (a) The photocatalysis mechanism for Cr(VI) reduction and BPA degradation over type II S–TiO_2/UiO-66-NH_2 heterojunction (Li et al., 2020b); (b) The mechanism of the photocatalytic Cr(VI) reduction over Z-scheme g-C_3N_4/UiO-66 heterojunction (Yi et al., 2019). (c) The most stable structure of g-C_3N_4 on UiO-66 surface after geometry relaxation (The green, brown, light blue and red spheres represent Zr, C, N and O atoms, respectively). (d) The electron density difference of carbon atoms UiO-66 and g-C_3N_4 in g-C_3N_4/UiO-66 heterojunction from the top view (The yellow and the blue regions represent increasing and decreasing of the electron density, respectively) (Yi et al., 2019). (For interpretation of the references to color in this figure legend, the reader is referred to the Web version of this article.)

composites can be expected to form between UiO-66 and *g*-C_3N_4 based on their HOMO/LUMO and CB/VB positions (Fig. 2b). However, some solid evidence (like XPS determination, active species identification) affirmed that the formed heterojunction is Z-scheme rather than the expected type II. Also, the DFT calculation was adopted to further clarify the flow direction of the photo-induced electrons. It was observed that in the as-prepared g-C_3N_4/UiO-66, the electron density around carbon atoms on UiO-66 was lower than that of the pristine UiO-66 (Fig. 2c and d), and the electron density around carbon and nitrogen atoms of the g-C_3N_4 was higher than those of the individual g-C_3N_4 (Yi et al., 2019). As well, the DFT calculation was affirmed as a powerful tool to determine the heterojunction types in other works (Wei et al., 2021; Zhao et al., 2021b). It was believed that the Z-scheme composite can achieve the photoinduced charge carriers with stronger redox ability on two components to boost the photocatalysis performance (Huang et al., 2017).

Besides the above-mentioned proofs like XPS determination and active species identification, the combination of DFT calculation and Pt or PbO_2 deposition test can further clarify the charge transfer tracking between the components. It was deemed that Pt^{4+} in the H_2PtCl_6 can be reduced into Pt^0 nanoparticles by the excessive photo-induced electrons, and the Pb^{2+} can be oxidized into PbO_2 nanoparticles by the accumulative holes, which can be used to monitor the electron and hole flow (Jiang et al., 2018). It can be observed that the Pt^0 nanoparticles were primarily deposited on the NH_2-UiO-66 octahedron in the Bi_5O_7-I/NH_2-UiO-66 heterojunction (Fig. 3a) (Zhao et al., 2021b). Detailly, the photo-induced electrons were accumulated on the LUMO of NH_2-UiO-66 as the holes on its HOMO were consumed by the electrons excited from the Bi_5O_7I via Z-scheme mechanism (Zhao et al., 2021b). The Z-scheme charge carriers transfer process was affirmed by DFT calculation, in which the average 0.2026 electrons were transferred from Bi_5O_7I to NH_2-UiO-66 at their interface (Fig. 3b). In our another case, the photo-deposition of PbO_2 NPs over WO_3/MIL-100(Fe) resulted from that the accumulative photo-generated holes left over the VB of the WO_3 led to the production of PbO_2 nanoparticles from Pb^{2+} (Fig. 3c) (Wang et al.,

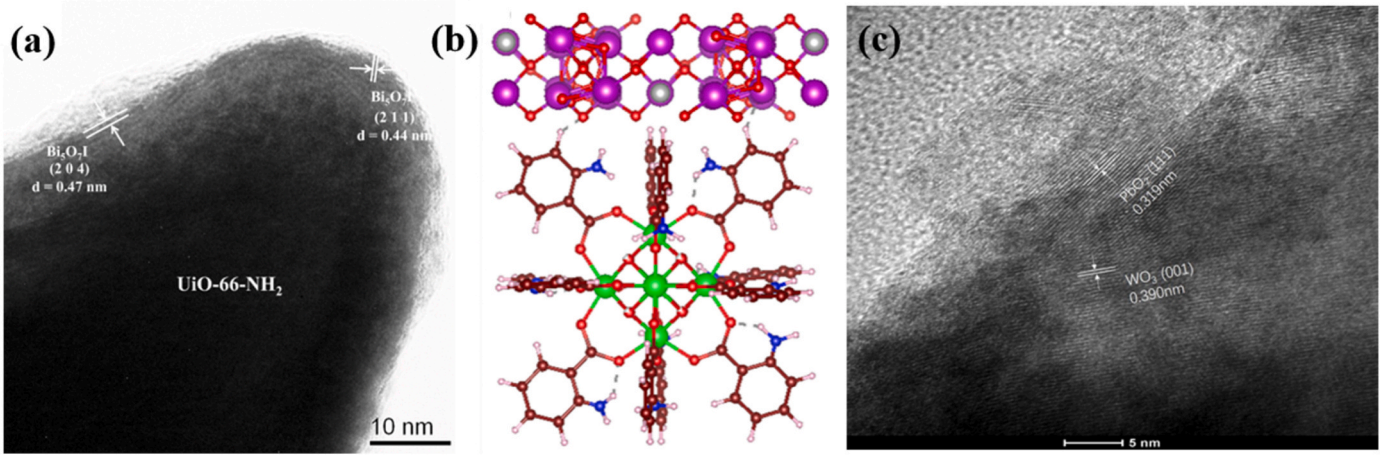

Fig. 3. (a) HRTEM image of photo-deposited Pt nanoparticles over the BU-5. (b) optimized structure model of the Bi_5O_7I/UiO-66-NH_2 heterojunction. The brown, blue, red, pink, green, purple, and grey spheres represent the C, N, O, H, Zr, Bi and I atoms, respectively (For interpretation of the references to color in this figure legend, the reader is referred to the Web version of this article.) (Zhao et al., 2021b), (c) HRTEM images of photo-deposited PbO_2 over M80W120 (Wang et al., 2021b).

2021b).

Some solid mediators like Au, Ag, and Cu could be introduced to construct the solid mediator Z-scheme photocatalysts for boosting the photocatalytic performances (Lai and Lee, 2021; Li et al., 2016). Our group fabricated a solid mediator Z-scheme Ag/Ag_3PO_4/NH_2-MIL-125 photocatalysts adopting the photo chemical reduction deposition strategy (Zhou et al., 2020b). Under the irradiation of visible light, the formed electrons over the conduction band (CB) of Ag_3PO_4 can be transported to the Ag^0 nanoparticles (NPs) via the Schottky barrier due to that the Fermi level of Ag^0 NPs is higher than the CB of Ag_3PO_4. As well, the produced holes on the highest occupied molecular orbital (HOMO) of NH_2-MIL-125 may migrate into the Ag^0 NPs, as the HOMO of NH_2-MIL-125 is more positive than the Fermi level of Ag^0 NPs (Fig. 4a). The proposed photocatalysis mechanism was further affirmed by the photo-deposition Pt^0 element experiment, in which the Pt^{4+} in the Cl_6H_2Pt was reduced into the Pt^0 by the electrons accumulated on the LUMO of NH_2-MIL-125 (Fig. 4b and **c**).

Besides being adopted as solid mediator Z-scheme photocatalysts, the precious metals like Ag and Pd nanoparticles can be coated on the MOFs to accomplish boosted separation of photo-induced charge carriers and enhanced visible-light absorption activity (Shen et al., 2013b; Zhang et al., 2019). Our group deposited Ag nanoparticles on NH_2-UiO-66 to produce Ag–NH_2-UiO-66 composites from $AgNO_3$ and NH_2-UiO-66 as precursors under high power Xe lamp, which demonstrated superior Cr(VI) reduction to the pristine NH_2-UiO-66 due to the improved charge carrier transfer at the interface (Zhou et al., 2020b).

Considering that MOF-derivatives might maintain the advantages of the MOF precursors like adjustable pore and flexible designability (Hang et al., 2022; Li et al., 2021; Zhang et al., 2021; Zhao et al., 2020a), a new approach was proposed to fabricate MOF-derivative/MOF composites like In_2S_3@NH_2-MIL-68(In)@In_2S_3 (Hou et al., 2020) and NH_2-MIL-125@TiO_2 (Zhang et al., 2018b) heterojunctions. Our group obtained marigold-flower-like TiO_2/MIL-125 composite (Fig. 5) adopting in-situ post-solvothermal treatment strategy to partially derivate MIL-125 with the aid of thioacetamide (Li et al., 2021). It was expected that the core-shell TiO_2/MIL-125 composite as type-II photocatalyst exhibited better photocatalytic Cr(VI) reduction activity than both the completely derived TiO_2 from MIL-125 and the pristine MIL-125.

2.3. The MOFs composites for simultaneously photocatalytic Cr(VI) reduction and adsorptive Cr(III) removal

It was well known that the accumulative formed Cr(III) in the system might inhibit the forward reaction from Cr(VI) to Cr(III) and result into masking the active sites by the potentially formed $Cr(OH)_3$ precipitates. Different from the expectation of red-shift of exciting light via introducing different visible light responsive semiconductor photocatalysts,

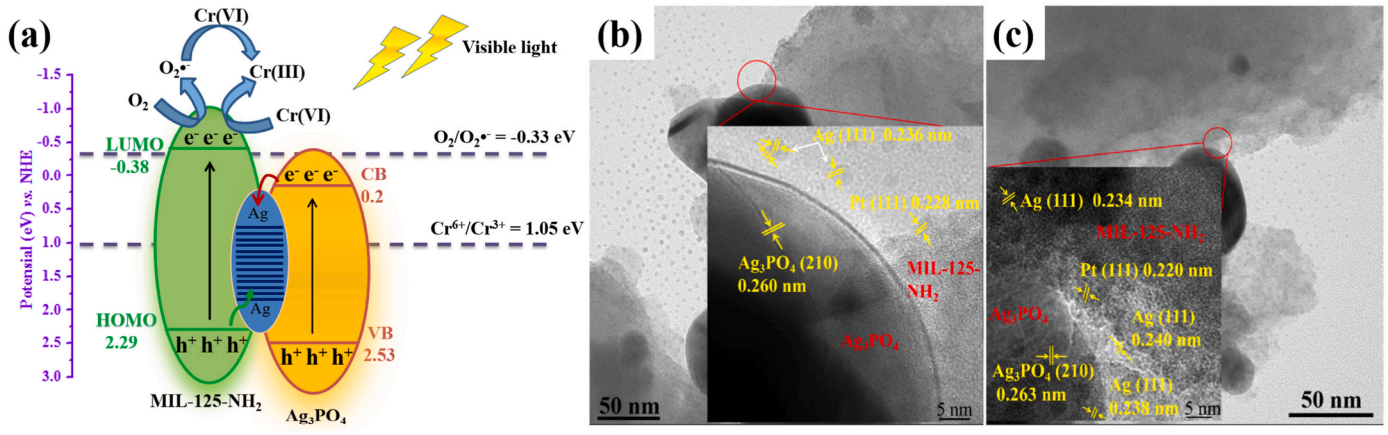

Fig. 4. (a) Schematic illustration and the proposed mechanism of photocatalytic Cr(VI) cleanup over AAMN-120 under visible light irradiation, (b) and (c) HRTEM image of Pt-loaded AAMN-120 (inserted figure is HRTEM of corresponding TEM area) (Zhou et al., 2020b).

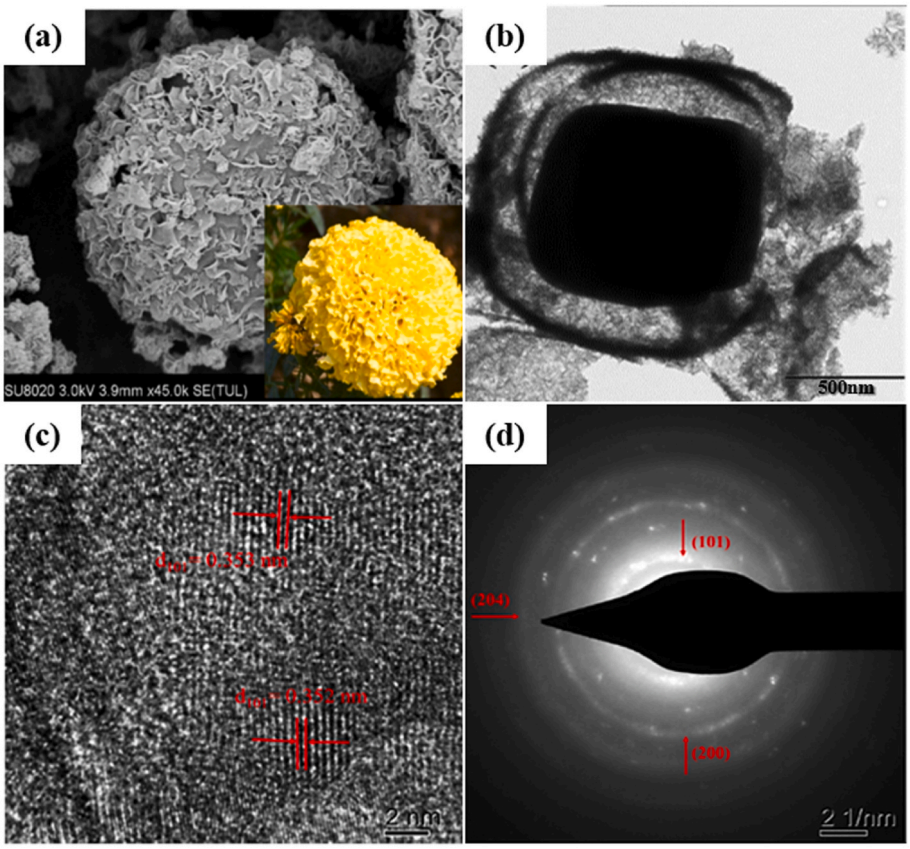

Fig. 5. (a) SEM images of TiO_2/MIL-125 (MT) and Inca marigold (inset), (b) TEM image of MIL-125, (c) HRTEM and (d) SAED of TiO_2 shell in MT (Li et al., 2021).

our group selected titanate nanotubes (TNTs), an effective and emerging adsorbent toward different cationic heavy metals (Liu et al., 2013, 2014, 2016), to fabricate TNT/BUC-21 composite for the simultaneous photocatalytic Cr(VI) reduction and adsorptive Cr(III) removal (Wang et al., 2019). The introduced TNTs could effectively capture the formed Cr(III) ions to push the forward reaction of Cr(VI) reduction and to avoid the formation of $Cr(OH)_3$ precipitates (Fig. 6a). It was observed that the TNTs can boost the Cr(VI) reduction (Fig. 6b and c) and total Cr removal (Fig. 6d) performances due to that TNT can adsorb the produced Cr(III) via both the electrostatic attractions and ion exchange (Fig. 6a). BUC-21 can reduce Cr(VI) and TNT can adsorb the formed Cr(III) under higher pH (like 5.0–9.0), which achieved perfect match of BUC-21 and TNT to construct bifunctional TNT/BUC-21 composite for simultaneously photocatalytic Cr(VI) reduction and adsorptive Cr(III) removal.

3. From powder MOFs for batch experiment to immobilized ones for continuous operation

The powder photocatalysts can offer sufficient contact interface and facilitate mass transport process of the wastewater pollutants (Liu et al., 2021). However, they are suffering from the difficult recovery/recycling in aqueous solution (Du et al., 2022). Some special reactors applicable to powder photocatalysts were designed and adopted to conduct photocatalysis process, however, massive energy should be input to press the water molecules through the membrane and retain the photocatalyst particles in the reactor (Wang et al., 2021a). To overcome the disadvantages like difficult recovery and reuse, it was feasible to immobilize MOF photocatalysts on some substrates like sand particles (Sadeghian et al., 2021), cellulosic foam (Liu et al., 2021), polymer composite bead (Valizadeh et al., 2020), and α-Al_2O_3 sheet (Du et al., 2019; Zhao et al., 2022).

Our group prepared the NH_2-UiO-66(Zr/Hf) membranes on the α-Al_2O_3 sheet using a reactive seeding strategy, which were adopted to accomplish photocatalytic Cr(VI) reduction under the illumination of sunlight (Du et al., 2019). The results revealed that the as-prepared NH_2-UiO-66(Zr) and NH_2-UiO-66(Hf) membranes displayed Cr(VI) reduction (initial concentration being 5.0 mg/L) efficiencies of >98.0% within 120 min. Moreover, the photocatalytic Cr(VI) reduction efficiencies of the NH_2-UiO-66(Zr) membrane maintained >94.0% during the continuous 20 runs' operation up to 2400.0 min (Fig. 7a). Even when the photocatalytic Cr(VI) reduction tests were carried out in the simulated wastewater containing Cr(VI) under the real sunlight, >93.0% reduction efficiency was accomplished, indicating the potential application for the real wastewater under the real sunlight. As well, the as-prepared NH_2-UiO-66(Zr) membrane demonstrated good water stability during the long-term operation, which was affirmed by the perfect octahedron morphology of the used NH_2-UiO-66(Zr) for 20 runs (Fig. 7b).

Inspired by the successfully photocatalytic Cr(VI) reduction of the NH_2-UiO-66(Zr) membrane, our group continued to immobilize NH_2-MIL-101(Fe) onto α-Al_2O_3 sheet to construct NH_2-MIL-101(Fe)@Al_2O_3 (MA) (Zhao et al., 2022). Different from the previous NH_2-UiO-66(Zr) membrane on Al_2O_3 sheet, it was difficult to observe the clear morphology of NH_2-MIL-101(Fe) in MA (Zhao et al., 2022). Therefore, the SEM-mapping, HRTEM-mapping, AFM and XPS analysis associated with argon ion etching were adopted to affirm the immobilization of NH_2-MIL-101(Fe) in MA. The as-prepared MA demonstrated outstanding photocatalytic Cr(VI) reduction performance adopting oxalic acid as hole consumer under white light irradiation, in which 100% Cr(VI) with initial concentration being 5.0 mg/L can be reduced into Cr(III) for 20 runs' operation within 400 min (20 min each run), as displayed in Fig. 8a. The continuous Cr(VI) reduction was also tested, and the results revealed that 100% Cr(VI) with initial concentration of 5 mg/L can be eliminated under white light up to 30 h (Fig. 8b). Also, the

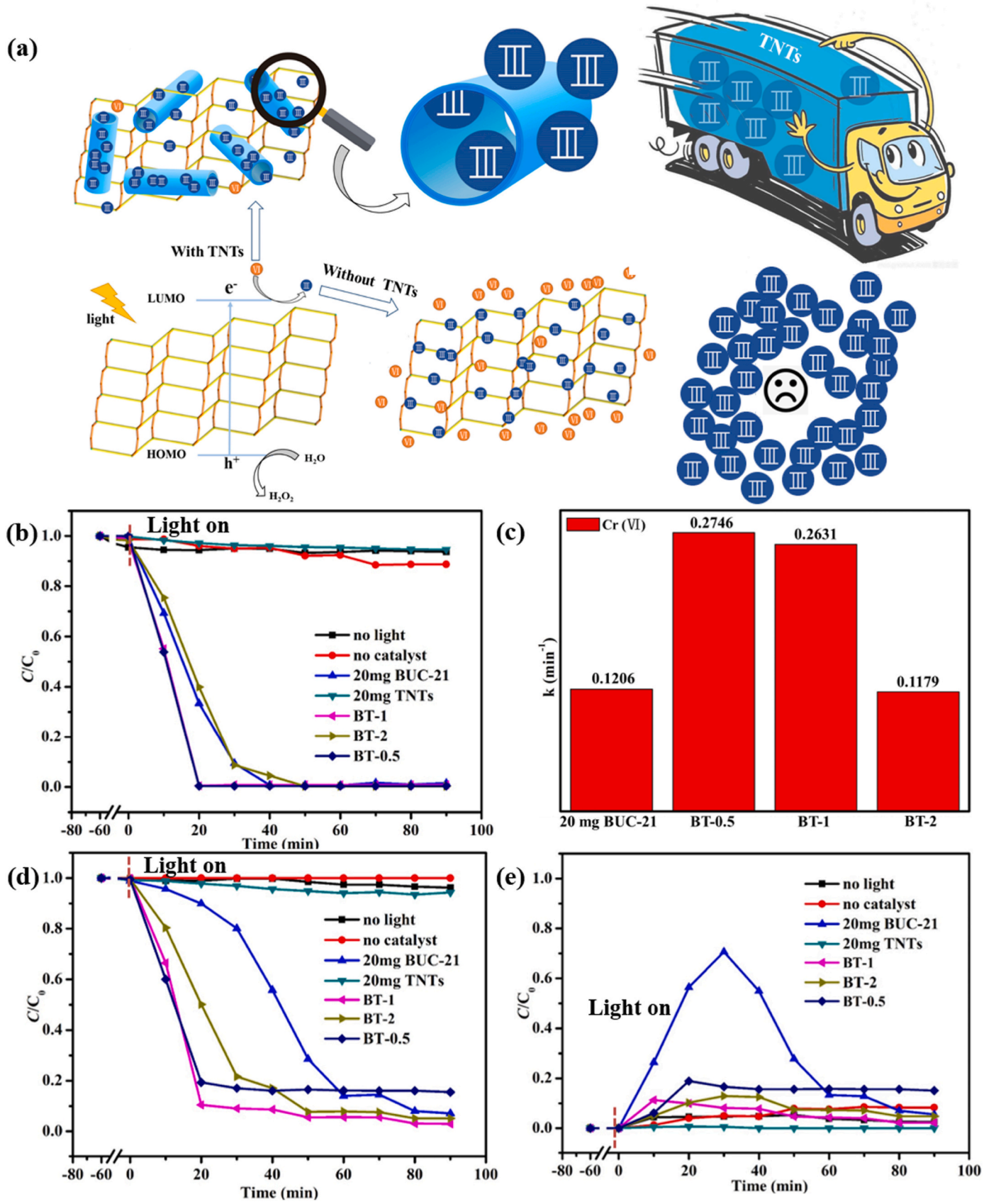

Fig. 6. (a) The simultaneous photocatalytic Cr(VI) reduction and adsorptive Cr(III) removal mechanisms over TNT/BUC-21 composite, (b) efficiencies of photocatalytic Cr(VI) reduction, (c) the corresponding reaction rate constants (k) and (d) Cr(VI) removal efficiencies of control experiments and with different photocatalysts (Wang et al., 2019).

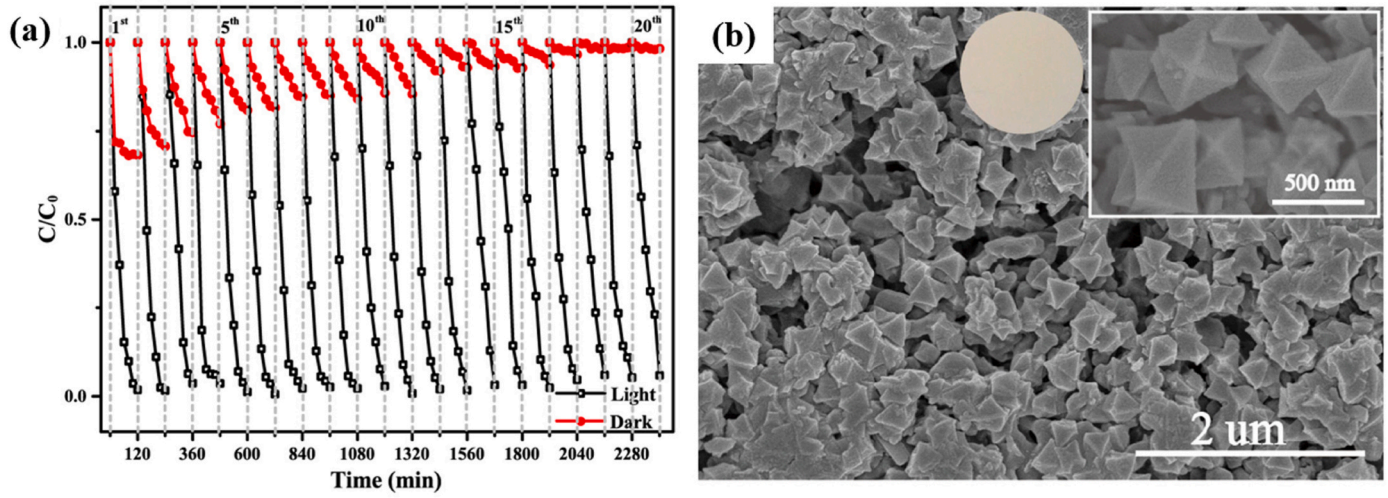

Fig. 7. (a) The long term (20 successive cycles for 2400 min) photocatalytic Cr(VI) reduction performances of the NH_2-UiO-66(Zr) membrane under the irradiation of the simulated sunlight. (Note: the red line in the figure is for the adsorption activities of the as-prepared membrane); (b) the octahedron morphology of the NH_2-UiO-66(Zr) in the used membrane after 20 runs' operation (Du et al., 2019). (For interpretation of the references to color in this figure legend, the reader is referred to the Web version of this article.)

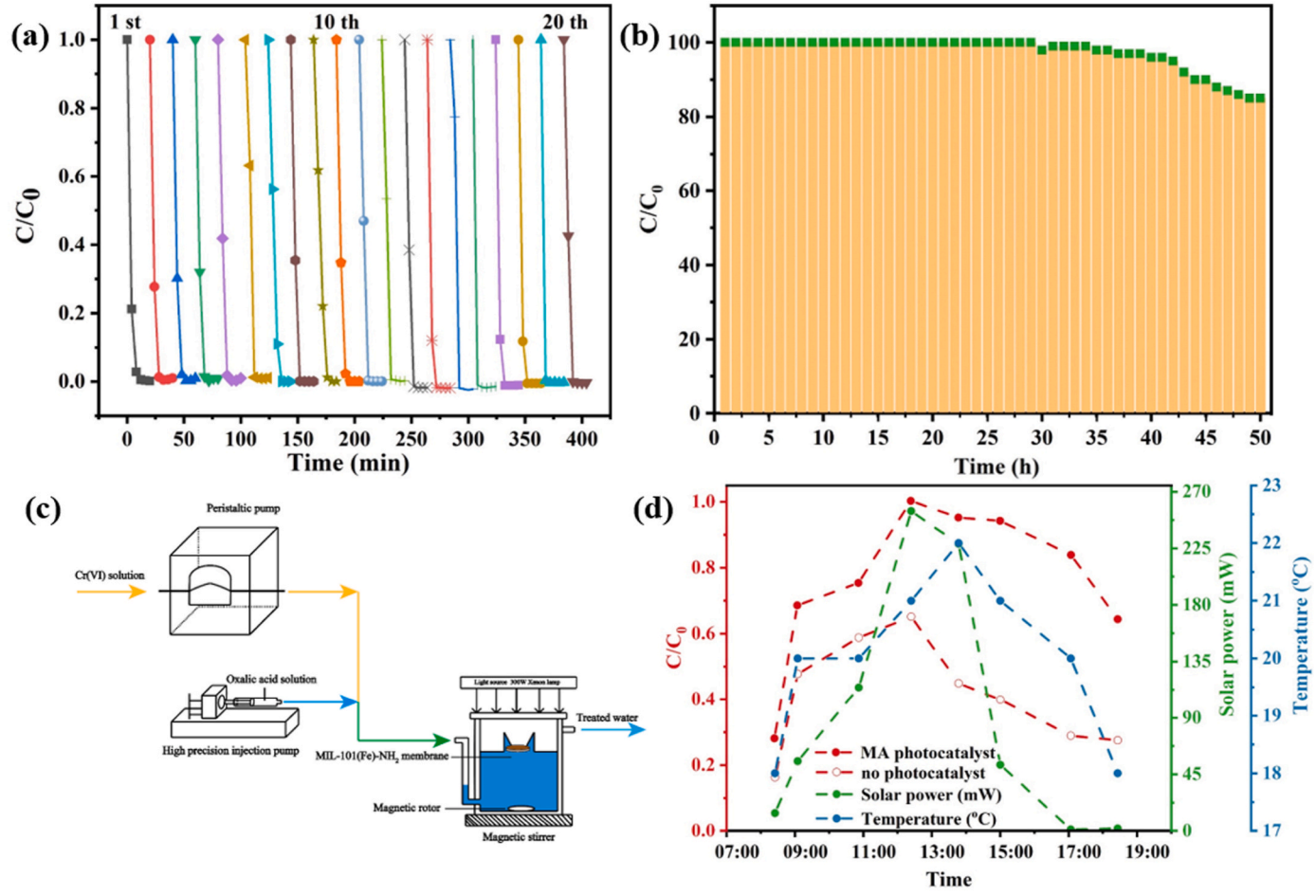

Fig. 8. (a) The long term (20 successive cycles for 400 min) photocatalytic Cr(VI) reduction performances of MA under the irradiation of white light in batch-scale, (b) the continuous Cr(VI) reduction performance of MA in fixed bed reactor, (c) the illustration of the fixed bed reactor for the continuous Cr(VI) reduction test and (d) the continuous Cr(VI) reduction under real sunlight from 8:00 a.m. to 6:00 p.m. Reaction conditions: the actual MIL-101(Fe)–NH_2 being ca. 15.0 mg per sheet, Cr (VI) = 5 mg/L, oxalic acid = 0.8 mM (batch test) and 20 mM (continuous test), 300 W white light irradiation, initial solution pH = 3.4 (Zhao et al., 2022).

continuous Cr(VI) reduction was achieved under real solar light, in which 100% Cr(VI) reduction efficiency was accomplished as the optical power reaching 280.3 mW at 12:00 (Fig. 8c and d). This work implied that the continuous operation adopting MA as photocatalyst in self-developed fixed bed reactor with oxalic acid as hole capturer under both white light and real solar light was feasible and promising.

4. The influence factors of the environmental applications

In recent years, increasing researchers focused on the potentially practical applications of photocatalytic Cr(VI) reduction (Ge et al., 2021; Zhang et al., 2017), in which it was essential to consider the influence of the pH, co-existing inorganic ions and organic matters (Hu et al., 2019).

4.1. The influence of pH

It was well known that pH might exert noticeable influence toward the surface charge (Zeta potential) of the photocatalysts (Ji et al., 2022) and the chemical species of Cr(VI) (Zhang et al., 2022), which can further alter the adsorptive interactions and the photocatalytic Cr(VI) reduction mechanism. Under the different pH conditions, the Cr(VI) displays various forms like CrO_4^{2-}, $Cr_2O_7^{2-}$, H_2CrO_4 and $HCrO_4^-$ (Fig. 9) (Li et al., 2021c; Zhao et al., 1998). As 2.0 < pH < 6.0, Cr(VI) exists primarily as $HCrO_4^-$ and $Cr_2O_7^{2-}$. The photocatalytic Cr(VI) reduction reactions followed the Eqs. (1) and (2) under acidic conditions, in which the excessive H^+ might facilitate the reduction from Cr(VI) to Cr(III) (Yi et al., 2019; Zhao et al., 2020b; Zhou et al., 2020b). While, as pH > 7.0, the CrO_4^{2-} is the primary specie, leading to a reduction reaction as expressed in Eq. (3) (Li et al., 2020a), in which the $Cr(OH)_3$ precipitate might be formed to mask the active sites over the photocatalysts. Thus, it was preferred that the photocatalytic Cr(VI) reduction was carried out under acidic conditions. However, the acidic reaction conditions required the photocatalysts to possess the property of acid-proof. Some MOFs like UiOs and MILs constructed from *hard* metal ions like Zr^{4+}, Ti^{4+}, and Fe^{3+} and organic carboxylate ligands are stable in the acid environment, which can be used as photocatalysts to conduct Cr(VI) reduction following the Eqs. (1) and (2). However, some MOFs composed of soft metal ions like Zn^{2+} and Co^{2+} and imidazolate were not suitable to reduce Cr(VI) to Cr(III) under acidic condition due to that they can be destroyed.

$$Cr_2O_7^{2-} + 14H^+ + 6e^- \rightarrow 2Cr^{3+} + 7H_2O \quad (1)$$

$$HCrO_4^- + 7H^+ + 3e^- \rightarrow Cr^{3+} + 4H_2O \quad (2)$$

$$CrO_4^{2-} + 4H_2O + 3e^- \rightarrow Cr(OH)_3 + 5OH^- \quad (3)$$

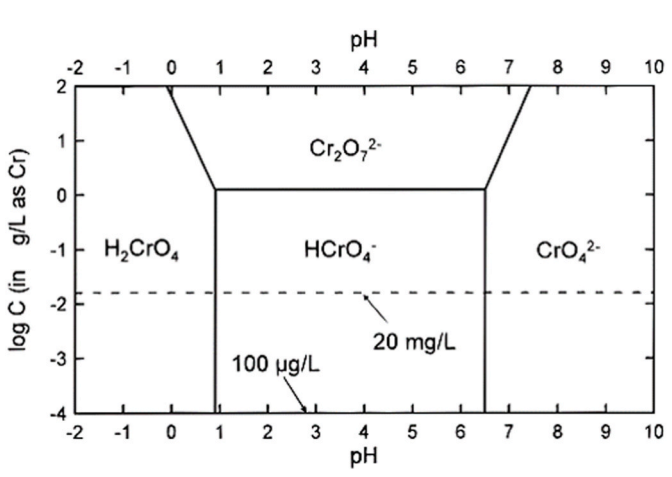

Fig. 9. Relative distribution of different Cr(VI) species in water as a function of pH and total Cr(VI) concentration (Zhao et al., 1998).

4.2. The influence of co-existing matters

The co-existing matters might influence the adsorption and reduction activities of the photocatalysts toward Cr(VI) (Yao et al., 2014). Generally, the photocatalysts with positive surface charge are inclined to attract the negative Cr(VI) ions to their active sites. The co-existing anions like Cl^-, NO_3^-, SO_4^{2-}, CO_3^{2-}, HCO_3^-, $H_nPO_4^{n-3}$ might compete with Cr(VI) to occupy the active sites. While, it was deemed that the co-existing cations like K^+, Na^+, Ca^{2+} and Mg^{2+} with stable electronic structures exerted negligible influence to the photocatalysis process considering that they would not to consume the photo-produced electrons or holes resulting from the stable and highest oxidation states (Li et al., 2022).

The Box-Behnken experimental design methodology was introduced to further clarify the influence of the co-existing matters on the Cr(VI) reduction process. In the Cr(VI) reduction system adopting BUC-21/$Bi_{24}O_{31}Br_{10}$ composite as photocatalyst (Zhao et al., 2020a), four influence variables like Cl^-, NO_3^-, SO_4^{2-} and DOM (dissolved organic matters) were selected to explore the influence toward photocatalysis activity. The ANOVA results revealed that the influence of the four variables on Cr(VI) reduction followed the order of DOM > NO_3^- > Cl^- > SO_4^{2-}. The optimum efficiency fitted by the Box-Behnken methodology demonstrated that the preferred concentrations of Cl^-, NO_3^-, SO_4^{2-} and DOM were 36.4, 9.5, 76.3 and 10.5 mg/L, respectively, which will provide useful information to adjust parameters for large-scale and practical Cr(VI) reduction application.

The influences of the co-existing organic matters varied under different photocatalysis systems. It was deemed that the organics acting as hole scavenger might consume the photo-induced holes, effectively inhibit the recombination of holes and electrons and supply more electron to reduce Cr(VI). Our group investigated the roles of tartaric acid > citric acid > oxalic acid toward the Cr(VI) performance of BUC-21/g-C_3N_4 composite photocatalyst, indicating that tartaric acid with two α-hydroxyl groups was inclined to consume the holes to achieve best Cr (VI) reduction performance (Gao et al., 2019). However, if the Cr(VI) reduction was originated from the superoxide radicals and electrons, the co-existing organics might inhibit the photocatalytic Cr(VI) reduction activity due to that the superoxide radicals might participate both the Cr (VI) reduction and organic oxidation (Li et al., 2020a; Wang et al., 2017).

In some photocatalysis systems like $(OH)_2$-UiO-66-20% photocatalyst (Li et al., 2021b), the introduced organics like tartaric acid can achieve "one stone killing three birds", i.e. consuming the photo-yielded electrons for enhanced separation of electron-hole pairs, reacting with photocatalyst to form charge-transfer-complex for boost the electron transfer, as well as producing $COO^{\cdot}$ radicals to directly participate the Cr(VI) reduction.

4.3. The influence of light

The light with different light intensities and wavelengths will provide different number of photons, which heavily influence the Cr(VI) reduction efficiencies. Generally, the increasing light intensity resulted into the increasing photons absorbed by the photocatalyst and the enhancing photocatalysis efficiency (Liu et al., 2009). Our group observed that both the Cr(VI) reduction efficiencies (40.7%, 76.7% and 99.9%) and rates (expressed as the pseudo-first-order kinetic constant of Cr(VI) reduction, 0.00492 ± 0.00027, 0.01381 ± 0.00092, and 0.06287 ± 0.00314 min^{-1}) increased with the stronger white light intensities (15.18, 24.25 and 46.07 mW/cm^2) (Zhao et al., 2020a). The apparent quantum efficiency (AQE), as a critical index to assess the photocatalysis performance, was introduced to test the influence of light with different wavelengths toward Cr(VI) reduction following Eq (4). Our group investigated the AQEs of S–TiO_2/NH_2-UiO-66 under the irradiation of

light with different wavelengths. The calculated AQEs were 0.56%, 0.48%, 0.33%, 0.05% and 0.04% at 315 nm, 330 nm, 365 nm, 380 nm, 400 nm and 420 nm, respectively, which corresponded perfectly to the plot trend of UV–vis DRS spectrum of S–TiO_2/NH_2-UiO-66. The investigation of the influences of light intensity and wavelength of the photocatalyst toward the Cr(VI) reduction can provide insight to the large-scale operation under special light or real sunlight (Jain et al., 2021).

$$\mathrm{AQE(Cr)} = \frac{3 \times [\text{number of reduced Cr(VI)}] \times hc}{Pt\lambda} \quad (4)$$

Where, P is the optical power, t is the irradiation time, λ is wavelength of light, and h and c are Planck constant ($h = 6.62607015 \times 10^{-34}$ J s) and light speed (299,792,458 m s^{-1}), respectively.

5. Conclusion and outlooks

We once proposed some challenges (i.e. how to improve the stability and electronic conductivity) in the previous review paper concerning Cr (VI) reduction adopting MOFs-based materials as photocatalysts. In the past five years, our research findings revealed that it was a feasible and effective strategy to improve the stability via immobilizing the MOFs on the substrate, which can accomplish continuous and long-term operation. In the future, more efforts should be put to immobilize uniform and nano-sized MOFs on the different large-sized substrates, considering the substrate-MOF interactions. Up to now, increasing findings demonstrated that the introduction of secondary semiconductor or even conductor to fabricate the composites with MOFs was successful to overcome the shortcoming of poor electronic conductivity. Especially, some organic conductor polymers like polyaniline (PANI) were adopted to not only enhance the electronic conductivity but also facilitate the shaping (film preparation, electrospinning).

Generally, Cr(VI) can be reduced into Cr(III) directly by photo-induced electrons, in which the superoxide radicals originated from the interaction between photo-yielded electron and dissolved oxygen might also sideways participate in reduction process. The introduction of organics to the photocatalytic Cr(VI) system might consume the formed holes to inhibit the re-combination of the charge carries. Especially, besides as hole scavenger and reductant, some co-existing organics like tartaric acid, citric acid and oxalic acid can form charge-transfer-complex for electron transfer and even produce $COO^{\cdot-}$ radicals to improve the Cr(VI) reduction. From this point, it was necessary consider the compositions of the real wastewater containing Cr(VI) to select suitable MOFs photocatalysts for simultaneous removal of Cr(VI) and organics in the future work.

It was ideal to use the abundant solar light as light source to achieve effective photocatalysis. Some approaches and efforts were used to develop visible light responsive photocatalyst. However, the poor light transmittance in the aqueous solution is a big obstacle. Also, it was awkward to observe that both the photocatalysis efficiency and rate decreased significantly once the light source was shifted from the UV light to the visible light (or real solar light). It was worthy to noting that the commercially available UV light even vacuum UV and short-wave UV (UVC) can provide stronger light intensity and shorter light wavelength to achieve more effective and rapid photocatalysis. From this point, it was important to design and manufacture suitable photocatalytic reactors for water treatment, taking account of various emerging photocatalysts and different light source.

Author contribution statement

Chong-Chen Wang: Conceptualization, Writing – original draft, Funding acquisition, Supervision, Project administration, Writing – review & editing. **Xueying Ren**: Resources, Writing – original draft. **Peng Wang**: Writing – review & editing. **Cheng Chang**: Resources

Declaration of competing interest

The authors declare that they have no known competing financial interests or personal relationships that could have appeared to influence the work reported in this paper.

Acknowledgments

This work was supported by National Natural Science Foundation of China (5187802), Beijing Talent Project (2020A27) and BUCEA Post Graduate Innovation Project (2021).

References

Ali, M., Pervaiz, E., Noor, T., Rabi, O., Zahra, R., Yang, M., 2021. Recent advancements in MOF-based catalysts for applications in electrochemical and photoelectrochemical water splitting: a review. Int. J. Energy Res. 45, 1190–1226.
Cai, G., Zhang, W., Jiao, L., Yu, S.-H., Jiang, H.-L., 2017. Template-directed growth of well-aligned MOF arrays and derived self-supporting electrodes for water splitting. Inside Chem. 2, 791–802.
Chen, D.-D., Yi, X.-H., Ling, L., Wang, C.-C., Wang, P., 2020a. Photocatalytic Cr(VI) sequestration and photo-Fenton bisphenol A decomposition over white light responsive PANI/MIL-88A(Fe). Appl. Organomet. Chem. 34, e5795.
Chen, D.-D., Yi, X.-H., Zhao, C., Fu, H., Wang, P., Wang, C.-C., 2020b. Polyaniline modified MIL-100(Fe) for enhanced photocatalytic Cr(VI) reduction and tetracycline degradation under white light. Chemosphere 245, 125659.
Chen, N., Cao, S., Zhang, L., Peng, X., Wang, X., Ai, Z., Zhang, L., 2021. Structural dependent Cr (VI) adsorption and reduction of biochar: hydrochar versus pyrochar. Sci. Total Environ. 783, 147084.
Ding, M., Cai, X., Jiang, H.-L., 2019. Improving MOF stability: approaches and applications. Chem. Sci. 10, 10209–10230.
Du, A., Fu, H., Wang, P., Zhao, C., Wang, C.-C., 2022. Enhanced catalytic peroxymonosulfate activation for sulfonamide antibiotics degradation over the supported CoS_x-CuS_x derived from ZIF-L(Co) immobilized on copper foam. J. Hazard Mater. 426, 128134.
Du, X.-D., Yi, X.-H., Wang, P., Zheng, W., Deng, J., Wang, C.-C., 2019. Robust photocatalytic reduction of Cr(VI) on UiO-66-NH_2(Zr/Hf) metal-organic framework membrane under sunlight irradiation. Chem. Eng. J. 356, 393–399.
Du, X., Yi, X., Wang, P., Deng, J., Wang, C.-C., 2019. Enhanced photocatalytic Cr(VI) reduction and diclofenac sodium degradation under simulated sunlight irradiation over MIL-100(Fe)/g-C_3N_4 heterojunctions. Chin. J. Catal. 40, 70–79.
Gao, Q., Lin, D., Fan, Y., He, Q., Wang, Q., 2019. Visible light induced photocatalytic reduction of Cr(VI) by self-assembled and amorphous Fe-2MI. Chem. Eng. J. 374, 10–19.
Ge, T., Jiang, Z., Shen, L., Li, J., Lu, Z., Zhang, Y., Wang, F., 2021. Synthesis and application of Fe_3O_4/$FeWO_4$ composite as an efficient and magnetically recoverable visible light-driven photocatalyst for the reduction of Cr (VI). Separ. Purif. Technol. 263, 118401.
Guo, Z., Zhao, H., Liu, X., Liang, X., Wei, H., Mei, Y., Xing, H., 2020. Construction of visible-light-responsive metal–organic framework with pillared structure for dye degradation and Cr(VI) reduction. Appl. Organomet. Chem. 34, e5487.
Hang, J., Yi, X.-H., Wang, C.-C., Fu, H., Wang, P., Zhao, Y., 2022. Heterogeneous photo-Fenton degradation toward sulfonamide matrix over magnetic Fe_3S_4 derived from MIL-100(Fe). J. Hazard Mater. 424, 127415.
He, Q., Fu, Y., Ge, X., Al-Enizi, A.M., Nafady, A., Wang, Q., Ma, S., 2021. Facile fabrication of Fe-BDC/Fe-2MI heterojunction with boosted photocatalytic activity for Cr(VI) reduction. J. Environ. Chem. Eng. 9, 105961.
Hou, Q., Li, X., Pi, Y., Xiao, J., 2020. Construction of In_2S_3@NH_2-MIL-68(In)@In_2S_3 sandwich homologous heterojunction for efficient CO_2 photoreduction. Ind. Eng. Chem. Res. 59, 20711–20718.
Hu, Y., Peng, X., Ai, Z., Jia, F., Zhang, L., 2019. Liquid nitrogen activation of zero-valent iron and its enhanced Cr (VI) removal performance. Environ. Sci. Technol. 53, 8333–8341.
Huang, Z.-F., Song, J., Wang, X., Pan, L., Li, K., Zhang, X., Wang, L., Zou, J.-J., 2017. Switching charge transfer of C_3N_4/$W_{18}O_{49}$ from type-II to Z-scheme by interfacial band bending for highly efficient photocatalytic hydrogen evolution. Nano Energy 40, 308–316.
Jain, A., Kumar, A., Kaur, H., Krishnan, V., 2021. Strategic combination of ultra violet-visible-near infrared light active materials towards maximum utilization of full solar spectrum for photocatalytic chromium reduction. Chemosphere 267, 128884.
Ji, Q., Cheng, X., Kong, X., Sun, D., Wu, Y., Xu, Z., Liu, Y., Duan, X., He, H., Li, S., 2022. Visible-light activation of persulfate ions by Z-scheme perylene diimide/MIL-101 (Cr) heterojunction photocatalyst towards efficient degradation of iohexol. Chem. Eng. J. 435, 134947.
Jiang, W., Zong, X., An, L., Hua, S., Miao, X., Luan, S., Wen, Y., Tao, F.F., Sun, Z., 2018. Consciously constructing heterojunction or direct Z-scheme photocatalysts by regulating electron flow direction. ACS Catal. 8, 2209–2217.
Kaur, H., Sinha, S., Krishnan, V., Koner, R.R., 2020. Photocatalytic reduction and recognition of Cr(VI): new Zn(II)-Based metal–organic framework as catalytic surface. Ind. Eng. Chem. Res. 59, 8538–8550.
Kaur, H., Sinha, S., Krishnan, V., Koner, R.R., 2021. Coordination networks for the recognition of oxo-anions. Dalton Trans. 50, 8273–8291.

Kumar, V., Singh, V., Kim, K.-H., Kwon, E.E., Younis, S.A., 2021. Metal-organic frameworks for photocatalytic detoxification of chromium and uranium in water. Coord. Chem. Rev. 447, 214148.
Lai, Y.-J., Lee, D.-J., 2021. Solid mediator Z-scheme heterojunction photocatalysis for pollutant oxidation in water: principles and synthesis perspectives. J. Taiwan Inst. Chem. Eng. 125, 88–114.
Li, H., Tu, W., Zhou, Y., Zou, Z., 2016. Z-scheme photocatalytic systems for promoting photocatalytic performance: recent progress and future challenges. Adv. Sci. 3, 1500389.
Li, J., Peng, T., Zhang, Y., Zhou, C., Zhu, A., 2018. Polyaniline modified SnO_2 nanoparticles for efficient photocatalytic reduction of aqueous Cr (VI) under visible light. Separ. Purif. Technol. 201, 120–129.
Li, N., He, M., Lu, X., Yan, B., Duan, X., Chen, G., Wang, S., 2022. Municipal solid waste derived biochars for wastewater treatment: production, properties and applications. Resour. Conserv. Recycl. 177, 106003.
Li, R., Chen, T., Pan, X., 2021a. Metal–organic-Framework-based materials for antimicrobial applications. ACS Nano 15, 3808–3848.
Li, Y.-H., Yi, X.-H., Li, Y.-X., Wang, C.-C., Wang, P., Zhao, C., Zheng, W., 2021b. Robust Cr(VI) reduction over hydroxyl modified UiO-66 photocatalyst constructed from mixed ligands: performances and mechanism insight with or without tartaric acid. Environ. Res. 201, 111596.
Li, Y.-X., Fu, H., Wang, P., Zhao, C., Liu, W., Wang, C.-C., 2020a. Porous tube-like ZnS derived from rod-like ZIF-L for photocatalytic Cr(VI) reduction and organic pollutants degradation. Environ. Pollut. 256, 113417.
Li, Y.-X., Han, Y.-C., Wang, C.-C., 2021c. Fabrication strategies and Cr(VI) elimination activities of the MOF-derivatives and their composites. Chem. Eng. J. 405, 126648.
Li, Y.-X., Wang, C.-C., Fu, H., Wang, P., 2021. Marigold-flower-like TiO_2/MIL-125 core−shell composite for enhanced photocatalytic Cr(VI) reduction. J. Environ. Chem. Eng. 9, 105451.
Li, Y.-X., Wang, X., Wang, C.-C., Fu, H., Liu, Y., Wang, P., Zhao, C., 2020b. S-TiO_2/UiO-66-NH_2 composite for boosted photocatalytic Cr(VI) reduction and bisphenol A degradation under LED visible light. J. Hazard Mater. 399, 123085.
Liang, R., Jing, F., Shen, L., Qin, N., Wu, L., 2015a. MIL-53(Fe) as a highly efficient bifunctional photocatalyst for the simultaneous reduction of Cr(VI) and oxidation of dyes. J. Hazard Mater. 287, 364–372.
Liang, R., Shen, L., Jing, F., Wu, W., Qin, N., Lin, R., Wu, L., 2015b. NH_2-mediated indium metal–organic framework as a novel visible-light-driven photocatalyst for reduction of the aqueous Cr(VI). Appl. Catal., B 162, 245–251.
Liu, J., Hao, D., Sun, H., Li, Y., Han, J., Fu, B., Zhou, J., 2021. Integration of MIL-101-NH_2 into cellulosic foams for efficient Cr(VI) reduction under visible light. Ind. Eng. Chem. Res. 60, 12220–12227.
Liu, W., Ni, J., Yin, X., 2014. Synergy of photocatalysis and adsorption for simultaneous removal of Cr(VI) and Cr(III) with TiO_2 and titanate nanotubes. Water Res. 53, 12–25.
Liu, W., Wang, T., Borthwick, A.G.L., Wang, Y., Yin, X., Li, X., Ni, J., 2013. Adsorption of Pb^{2+}, Cd^{2+}, Cu^{2+} and Cr^{3+} onto titanate nanotubes: competition and effect of inorganic ions. Sci. Total Environ. 456–457, 171–180.
Liu, W., Zhao, X., Wang, T., Zhao, D., Ni, J., 2016. Adsorption of U(VI) by multilayer titanate nanotubes: effects of inorganic cations, carbonate and natural organic matter. Chem. Eng. J. 286, 427–435.
Liu, Y., Zhang, Y.C., Xu, X.F., 2009. Hydrothermal synthesis and photocatalytic activity of CdO_2 nanocrystals. J. Hazard Mater. 163, 1310–1314.
Ma, S.-Q., Yu, B., Yi, X.-H., Wang, C.-C., 2020. Two new Zn-based coordination polymers constructed from a light responsive organic ligand: efficient clean-up of Cr(VI) and organic pollutants. Polyhedron 188, 114701.
Sadeghian, S., Pourfakhar, H., Baghdadi, M., Aminzadeh, B., 2021. Application of sand particles modified with NH_2-MIL-101(Fe) as an efficient visible-light photocatalyst for Cr(VI) reduction. Chemosphere 268, 129365.
Shen, L., Liang, R., Luo, M., Jing, F., Wu, L., 2015. Electronic effects of ligand substitution on metal–organic framework photocatalysts: the case study of UiO-66. Phys. Chem. Chem. Phys. 17, 117–121.
Shen, L., Liang, S., Wu, W., Liang, R., Wu, L., 2013a. Multifunctional NH_2-mediated zirconium metal–organic framework as an efficient visible-light-driven photocatalyst for selective oxidation of alcohols and reduction of aqueous Cr(vi). Dalton Trans. 42, 13649–13657.
Shen, L., Wu, W., Liang, R., Lin, R., Wu, L., 2013b. Highly dispersed palladium nanoparticles anchored on UiO-66(NH_2) metal-organic framework as a reusable and dual functional visible-light-driven photocatalyst. Nanoscale 5, 9374–9382.
Shi, L., Wang, T., Zhang, H., Chang, K., Meng, X., Liu, H., Ye, J., 2015. An amine-functionalized iron(III) metal–organic framework as efficient visible-light photocatalyst for Cr(VI) reduction. Adv. Sci. 2, 1500006.
Valizadeh, B., Nguyen, T.N., Kampouri, S., Sun, D.T., Mensi, M.D., Stylianou, K., Smit, B., Queen, W.L., 2020. A novel integrated Cr(vi) adsorption–photoreduction system using MOF@polymer composite beads. J. Mater. Chem. 8, 9629–9637.
Wang, C.-C., Du, X.-D., Li, J., Guo, X.-X., Wang, P., Zhang, J., 2016. Photocatalytic Cr(VI) reduction in metal-organic frameworks: a mini-review. Appl. Catal., B 193, 198–216.
Wang, C.-C., Ho, Y.-S., 2016. Research trend of metal–organic frameworks: a bibliometric analysis. Scientometrics 109, 481–513.
Wang, C.-C., Li, J.-R., Lv, X.-L., Zhang, Y.-Q., Guo, G., 2014. Photocatalytic organic pollutants degradation in metal–organic frameworks. Energy Environ. Sci. 7, 2831–2867.
Wang, C.-C., Wang, X., Liu, W., 2020a. The synthesis strategies and photocatalytic performances of TiO_2/MOFs composites: a state-of-the-art review. Chem. Eng. J. 391, 123601.
Wang, C.-C., Yi, X.-H., Wang, P., 2019. Powerful combination of MOFs and C_3N_4 for enhanced photocatalytic performance. Appl. Catal., B 247, 24–48.
Wang, C.-C., Zhang, Y.-Q., Li, J., Wang, P., 2015a. Photocatalytic CO_2 reduction in metal–organic frameworks: a mini review. J. Mol. Struct. 1083, 127–136.
Wang, D., Mueses, M.A., Márquez, J.A.C., Machuca-Martínez, F., Grčić, I., Peralta Muniz Moreira, R., Li Puma, G., 2021a. Engineering and modeling perspectives on photocatalytic reactors for water treatment. Water Res. 202, 117421.
Wang, F.-X., Wang, C.-C., Du, X., Li, Y., Wang, F., Wang, P., 2022. Efficient removal of emerging organic contaminants via photo-Fenton process over micron-sized Fe-MOF sheet. Chem. Eng. J. 429, 132495.
Wang, F.-X., Yi, X.-H., Wang, C.-C., Deng, J.-G., 2017. Photocatalytic Cr(VI) reduction and organic-pollutant degradation in a stable 2D coordination polymer. Chin. J. Catal. 38, 2141–2149.
Wang, H., Yuan, X., Wu, Y., Zeng, G., Chen, X., Leng, L., Wu, Z., Jiang, L., Li, H., 2015b. Facile synthesis of amino-functionalized titanium metal-organic frameworks and their superior visible-light photocatalytic activity for Cr(VI) reduction. J. Hazard Mater. 286, 187–194.
Wang, J.-W., Qiu, F.-G., Wang, P., Ge, C., Wang, C.-C., 2021b. Boosted bisphenol A and Cr(VI) cleanup over Z-scheme WO_3/MIL-100(Fe) composites under visible light. J. Clean. Prod. 279, 123408.
Wang, Q., Gao, Q., Al-Enizi, A.M., Nafady, A., Ma, S., 2020b. Recent advances in MOF-based photocatalysis: environmental remediation under visible light. Inorg. Chem. Front. 7, 300–339.
Wang, X., Liu, W., Fu, H., Yi, X.-H., Wang, P., Zhao, C., Wang, C.-C., Zheng, W., 2019. Simultaneous Cr(VI) reduction and Cr(III) removal of bifunctional MOF/Titanate nanotube composites. Environ. Pollut. 249, 502–511.
Wang, Y., Su, Y., Fang, W., Zhang, Y., Li, X., Zhang, G., Sun, W., 2020c. SnO_2/SnS_2 nanocomposite anchored on nitrogen-doped RGO for improved photocatalytic reduction of aqueous Cr (VI). Powder Technol. 363, 337–348.
Wei, H., Zhang, Q., Zhang, Y., Yang, Z., Zhu, A., Dionysiou, D.D., 2016. Enhancement of the Cr(VI) adsorption and photocatalytic reduction activity of g-C_3N_4 by hydrothermal treatment in HNO_3 aqueous solution. Appl. Catal., A 521, 9–18.
Wei, X., Wang, C.-C., Li, Y., Wang, P., Wei, Q., 2021. The Z-scheme NH_2-UiO-66/PTCDA composite for enhanced photocatalytic Cr(VI) reduction under low-power LED visible light. Chemosphere 280, 130734.
Wei, X., Wang, P., Fu, H., Zhao, C., Wang, C.-C., 2020. Boosted photocatalytic elimination toward Cr(VI) and organic pollutants over BUC-21/$Cd_{0.5}Zn_{0.5S}$ under LED visible Light. Mater. Res. Bull. 129, 110903.
Wu, L., Wang, C.-C., Chu, H.-Y., Yi, X.-H., Wang, P., Zhao, C., Fu, H., 2021. Bisphenol A cleanup over MIL-100(Fe)/CoS composites: pivotal role of Fe–S bond in regenerating Fe^{2+} ions for boosted degradation performance. Chemosphere 280, 130659.
Xie, H., Ma, D., Liu, W., Chen, Q., Zhang, Y., Huang, J., Zhang, H., Jin, Z., Luo, T., Peng, F., 2020. Zr-Based MOFs as new photocatalysts for the rapid reduction of Cr (vi) in water. New J. Chem. 44, 7218–7225.
Xu, Q., Zhang, L., Cheng, B., Fan, J., Yu, J., 2020. S-scheme heterojunction photocatalyst. Inside Chem. 6, 1543–1559.
Yao, L., Zhang, Y.C., Li, J., Chen, Y., 2014. Photocatalytic properties of SnS_2/SnO_2 nanocomposite prepared by thermal oxidation of SnS_2 nanoparticles in air. Separ. Purif. Technol. 122, 1–5.
Yi, X.-H., Ji, H., Wang, C.-C., Li, Y., Li, Y.-H., Zhao, C., Wang, A., Fu, H., Wang, P., Zhao, X., Liu, W., 2021. Photocatalysis-activated SR-AOP over PDINH/MIL-88A(Fe) composites for boosted chloroquine phosphate degradation: performance, mechanism, pathway and DFT calculations. Appl. Catal., B 293, 120229.
Yi, X.-H., Ma, S.-Q., Du, X.-D., Zhao, C., Fu, H., Wang, P., Wang, C.-C., 2019. The facile fabrication of 2D/3D Z-scheme g-C_3N_4/UiO-66 heterojunction with enhanced photocatalytic Cr(VI) reduction performance under white light. Chem. Eng. J. 375, 121944.
Yi, X.-H., Wang, F.-X., Du, X.-D., Fu, H., Wang, C.-C., 2018. Highly efficient photocatalytic Cr(VI) reduction and organic pollutants degradation of two new bifunctional 2D Cd/Co-based MOFs. Polyhedron 152, 216–224.
Zeng, L., Guo, X., He, C., Duan, C., 2016. Metal–organic frameworks: versatile materials for heterogeneous photocatalysis. ACS Catal. 6, 7935–7947.
Zhang, B., Zhang, J., Tan, X., Shao, D., Shi, J., Zheng, L., Zhang, J., Yang, G., Han, B., 2018a. MIL-125-NH_2@TiO_2 core–shell particles produced by a post-solvothermal route for high-performance photocatalytic H_2 production. ACS Appl. Mater. Interfaces 10, 16418–16423.
Zhang, F., Zhang, Y., Wang, Y., Zhu, A., Zhang, Y., 2022. Efficient photocatalytic reduction of aqueous Cr (VI) by Zr^{4+} doped and polyaniline coupled SnS_2 nanoflakes. Separ. Purif. Technol. 283, 120161.
Zhang, F., Zhang, Y., Zhang, G., Yang, Z., Dionysiou, D.D., Zhu, A., 2018b. Exceptional synergistic enhancement of the photocatalytic activity of SnS_2 by coupling with polyaniline and N-doped reduced graphene oxide. Appl. Catal., B 236, 53–63.
Zhang, F., Zhang, Y., Zhou, C., Yang, Z., Xue, H., Dionysiou, D.D., 2017. A new high efficiency visible-light photocatalyst made of SnS_2 and conjugated derivative of polyvinyl alcohol and its application to Cr (VI) reduction. Chem. Eng. J. 324, 140–153.
Zhang, W., Wang, L., Zhang, J., 2019. Preparation of Ag/UiO-66-NH_2 and its application in photocatalytic reduction of Cr(VI) under visible light. Res. Chem. Intermed. 45, 4801–4811.
Zhang, X.-W., Wang, F., Wang, C.-C., Wang, P., Fu, H., Zhao, C., 2021. Photocatalysis activation of peroxodisulfate over the supported Fe_3O_4 catalyst derived from MIL-88A(Fe) for efficient tetracycline hydrochloride degradation. Chem. Eng. J. 426, 131927.
Zhang, Y., Zhang, Q., Shi, Q., Cai, Z., Yang, Z., 2015. Acid-treated g-C_3N_4 with improved photocatalytic performance in the reduction of aqueous Cr(VI) under visible-light. Separ. Purif. Technol. 142, 251–257.

Zhang, Y.C., Yang, M., Zhang, G., Dionysiou, D.D., 2013. HNO_3-involved one-step low temperature solvothermal synthesis of N-doped TiO_2 nanocrystals for efficient photocatalytic reduction of Cr (VI) in water. Appl. Catal., B 142, 249–258.
Zhao, C., Pan, X., Wang, Z., Wang, C.-C., 2021a. 1 + 1 > 2: a critical review of MOF/bismuth-based semiconductor composites for boosted photocatalysis. Chem. Eng. J. 417, 128022.
Zhao, C., Wang, J., Chen, X., Wang, Z., Ji, H., Chen, L., Liu, W., Wang, C.-C., 2021b. Bifunctional $Bi_{12}O_{17}Cl_2$/MIL-100(Fe) composites toward photocatalytic Cr(VI) sequestration and activation of persulfate for bisphenol A degradation. Sci. Total Environ. 752, 141901.
Zhao, C., Wang, Z., Chen, X., Chu, H., Fu, H., Wang, C.-C., 2020a. Robust photocatalytic benzene degradation using mesoporous disk-like N-TiO_2 derived from MIL-125(Ti). Chin. J. Catal. 41, 1186–1197.
Zhao, C., Wang, Z., Li, X., Yi, X., Chu, H., Chen, X., Wang, C.-C., 2020b. Facile fabrication of BUC-21/$Bi_{24}O_{31}Br_{10}$ composites for enhanced photocatalytic Cr(VI) reduction under white light. Chem. Eng. J. 389, 123431.
Zhao, D., SenGupta, A.K., Stewart, L., 1998. Selective removal of Cr(VI) oxyanions with a new anion exchanger. Ind. Eng. Chem. Res. 37, 4383–4387.
Zhao, H., Xia, Q., Xing, H., Chen, D., Wang, H., 2017. Construction of pillared-layer MOF as efficient visible-light photocatalysts for aqueous Cr(VI) reduction and dye degradation. ACS Sustain. Chem. Eng. 5, 4449–4456.
Zhao, Q., Wang, C.-C., Wang, P., 2022. Effective norfloxacin elimination via photo-Fenton process over the MIL-101(Fe)-NH_2 immobilized on α-Al_2O_3 sheet. Chin. Chem. Lett. https://doi.org/10.1016/j.cclet.2022.01.033.
Zhao, Z., An, H., Lin, J., Feng, M., Murugadoss, V., Ding, T., Liu, H., Shao, Q., Mai, X., Wang, N., Gu, H., Angaiah, S., Guo, Z., 2019. Progress on the photocatalytic reduction removal of chromium contamination. Chem. Rec. 19, 873–882.
Zheng, M., Zhao, X., Wang, K., She, Y., Gao, Z., 2019. Highly efficient removal of Cr(VI) on a stable metal–organic framework based on enhanced H-bond interaction. Ind. Eng. Chem. Res. 58, 23330–23337.
Zhong, J., Yi, X.-H., Wang, P., Wang, C.-C., 2019. A stable 1D mixed-valence Cu_I/Cu_{II} coordination polymer with photocatalytic reduction activity toward Cr(Ⅵ). J. Mol. Struct. 1183, 256–262.
Zhou, Y.-C., Wang, P., Fu, H., Zhao, C., Wang, C.-C., 2020a. Ternary Ag/Ag_3PO_4/MIL-125-NH_2 Z-scheme heterojunction for boosted photocatalytic Cr(VI) cleanup under visible light. Chin. Chem. Lett. 31, 2645–2650.
Zhou, Y.-C., Xu, X.-Y., Wang, P., Fu, H., Zhao, C., Wang, C.-C., 2019. Facile fabrication and enhanced photocatalytic performance of visible light responsive UiO-66-NH_2/Ag_2CO_3 composite. Chin. J. Catal. 40, 1912–1923.
Zhou, Y.C., Wang, C.-C., Wang, P., Fu, H.-F., Zhao, C., 2020b. In-Situ photochemical reduction of Ag-UiO-66-NH_2 composite for enhanced photocatalytic performance. Chin. J. Inorg. Chem. 36, 2100–2112.